Catal Lett (2009) 128:49–56
DOI 10.1007/s10562-008-9746-4

Dynamical Changes in the Cu–ZnO_x Interaction Observed in a Model Methanol Synthesis Catalyst

M. W. E. van den Berg · S. Polarz · O. P. Tkachenko · K. Kähler · M. Muhler · W. Grünert

Received: 29 August 2008 / Accepted: 21 October 2008 / Published online: 11 November 2008

Abstract A systematic series of model methanol synthesis catalysts was prepared by sequential impregnation of a mesoporous silica material (5 nm average pore size) with an organometallic ZnO precursor which is liquid at room temperature, followed by the infiltration with an aqueous Cu nitrate solution. These catalysts, which contained 14–20 wt.% Cu and 1–5 wt.% Zn, were characterized by N_2O reactive chemisorption, by EXAFS and by measuring their methanol synthesis activities. It was observed that the formation of confined, nanocrystalline ZnO prior to copper infiltration is of major importance for the development of catalyst activity. Severe reduction of properly prepared catalysts (10% CO/H_2, 673 K, 15 min) leads to the emergence of a new feature in the ZnK EXAFS spectrum which was assigned to a Cu neighbour by combined evidence from the ZnK EXAFS and XANES regions. The zinc oxide component was partially reduced as well, but Zn(0) was not formed to any significant extent. Catalysts which developed this Cu–Zn^{2+} interaction under severe reduction were superior in terms of methanol synthesis rate per m^2 Cu surface area to a sample which did not exhibit this feature.

M. W. E. van den Berg · K. Kähler · M. Muhler · W. Grünert (✉)
Lehrstuhl für Technische Chemie, Ruhr-Universität Bochum, P.O. Box 102148, 44780 Bochum, Germany
e-mail: w.gruenert@techem.ruhr-uni-bochum.de

S. Polarz
Chemistry Department, Konstanz University, Konstanz, Germany

O. P. Tkachenko
N. D. Zelinsky Institute of Organic Chemistry, Russian Academy of Sciences, Moscow, Russia

Keywords Methanol synthesis · Copper · Zinc oxide · Metal-support interaction · Model catalyst · Mesoporous silica · XAFS

1 Introduction

It is well known that the interaction between the active Cu component and the ZnO additive is essential for achieving a high activity of methanol synthesis catalysts, but the nature of this promoting effect is still a matter of debate. The manifestation of the Cu–ZnO_x interaction depends on the redox potential of the surrounding gas phase. The proposed explanations for the favourable influence observed under strongly reducing conditions include changes in the Cu particle morphology to preferential exposure of the most active (111) facets [1, 2], formation of an oxygen-deficient ZnO_x adlayer on copper, with higher activity of the Cu–ZnO_x interaction sites [3, 4], and crystal strain in the copper particles caused by inclusion of ZnO_x entities [5]. Progress in the differentiation between these models is difficult with catalysts of technical interest because these contain the Cu and ZnO component in particles of several nanometre size, in which the percentage of Zn (Cu) atoms that can be engaged in a mutual interaction via the particle surface is very small.

A promising idea is to confine the formation of ZnO and copper in such a way that the formation of Cu–ZnO contacts becomes unavoidable (Fig. 1). The use of mesoporous silica materials as confining reaction fields would be one way to achieve this goal [6]. However, it was found that the conversion of Zn^{2+}-salt precursors to ZnO in mesoporous silica fails due to the undesired formation of zinc silicate species [7, 8]. It could be shown that a route involving a special organometallic and liquid at room temperature

Fig. 1 Schematic representation of the synthetic approach used for the synthesis of Cu–ZnO_x model catalysts. The reaction of a special, organometallic precursor, a heterocubane $[MeZnOEtOMe]_4$ with water results in nanocrystalline ZnO with Wurtzite structure confined to the pores of mesoporous silica materials. Subsequently, different amounts of copper nitrate can be infiltrated into the porous materials. The spatial confinement is expected to lead to enhanced formation of Cu–ZnO_x contacts (shaded)

precursor prevents the zinc silicate formation, and nanocrystalline ZnO particles can be successfully grown inside the pores of mesoporous silica [9]. On this basis, model methanol synthesis catalysts were prepared by the infiltration of aqueous solutions of Cu^{2+} salts (nitrates or acetates) into the ZnO containing pores [8]. These catalysts exhibit appreciable methanol synthesis activity, inferior though to that of a commercial reference sample, but comparable or even better in terms of rate per m^2 Cu surface area. For the characterisation of the Cu–ZnO_x interaction we followed an observation described in [4] according to which methanol synthesis catalysts develop a transient excess activity after having been treated in CO at the reaction temperature for extended time. After a similar, somewhat more severe treatment, we noted a significant new shell in the ZnK EXAFS spectrum of a SiO_2-encapsulated Cu/ZnO catalyst [8]. An assignment of this shell was not possible at that stage due to its low intensity.

The present study aims at the development of samples that exhibit the new shell with higher intensity, which would permit its reliable interpretation. To this end, the composition of the samples was changed towards a large excess of Cu over Zn. On the basis of both EXAFS and XANES spectra of these catalysts, the new shell in the ZnK EXAFS could be assigned to copper, i.e., it arises from a direct Cu–Zn interaction. Its intensity increases with decreasing Zn content indicating that in catalysts of this type all Zn species can enter the interaction with the copper particles.

2 Experimental

2.1 Materials

The preparation of the matrix, which is a mesoporous silica of wormhole-type pore structure, has been described in detail in [9]. The average pore diameter is 50 Å, but the pore system is bicontinuous, with micropores connecting the mesopores. This matrix was loaded with the 'Zn_4O_4' heterocubane-type precursor ($[CH_3ZnOCH_2CH_2OCH_3]_4$ (I)) by liquid infiltration with a solution of (I) in *n*-pentane the concentration of which was chosen to achieve the desired Zn-content. The mesoporous silica materials containing the ZnO precursors were treated at $T = 60$ °C and a relative humidity of 50% in order to achieve ZnO formation. Then, the materials were dried in vacuum at $T = 80$ °C. Subsequently, Cu was introduced by conventional aqueous impregnation using a copper nitrate solution of appropriate concentration. Finally, the samples were dried in vacuum for 3 days. In Table 1, the samples used are introduced together with the labels employed for them in the present paper. The compositions were determined on the basis of the XAFS step heights, which has given results comparable to ICP analyses in earlier work [8]. The catalytic data will be referred to the activity of a commercial reference catalyst that contained ca. 50 wt.% Cu, 35 wt.% ZnO, and 15 wt.% Al_2O_3.

XAFS spectra (CuK edge–8.979 keV, ZnK edge–9.659 keV) were measured in transmission mode at Hasylab E4 station (Hamburg) using a Si(111) double crystal monochromator detuned to 50% of maximum intensity to exclude higher harmonics from the X-ray beam. Treatments were performed in an in situ EXAFS cell [10], and absorption spectra μ(E) were then taken at liquid nitrogen temperature. Initially, the samples were heated in flowing

Table 1 Cu–ZnO/SiO_2 samples used in the present study

Sample code	wt.% Cu[a]	wt.% Zn[a]	Cu surface area (m^2/g)
ZnCu-5/14	14.1	5.1	2.9
CuZn-15/5[b]	14.6	5.2	1.1
ZnCu-3/16	16.1	2.7	2.0
ZnCu-2/20	19.6	1.5	n.d.
ZnCu-1/19	18.9	0.9	2.0

[a] From EXAFS step height

[b] Reversed introduction of components into matrix—Cu first, then Zn

helium at ~423 K for 30 min in order to remove physisorbed water. The subsequent treatments, which will be compared in the following, are reduction at 523 K in a flow of 5% H_2/He, with a temperature ramp of 5 K/min to the reduction temperature and a 15 min isothermal period (R_H523), and reduction at 673 K in 10% CO/H_2 subsequent to R_H523, with a temperature ramp between 523 and 673 K of 5 K/min and a 15 min isothermal period ($R_{CO}673$). The data were processed with the software package VIPER [11]. Background subtraction was made using a Victoreen polynomial fitted to the pre-edge region. The atomic background μ_0 was estimated with a smoothing cubic spline, Fourier analysis of the k^2-weighted experimental function $\chi = (\mu - \mu_0)/\mu_0$ was made with a Kaiser window. For the determination of structural parameters, theoretical references calculated by the FEFF8.10 code [12] were used.

In samples containing a large Cu excess, the influence of the Cu EXAFS on the nearby Zn spectrum cannot be neglected, in particular when the copper is in the metallic state. To correct for this influence, the Cu features appearing above the ZnK edge were subtracted from the Zn spectra using the spectrum of a Cu foil attenuated by a factor to match the amplitudes in the CuK EXAFS of the corresponding catalyst. The error made in this simplified correction is not serious because it will be shown that the Cu particles were rather big in our samples and their dispersion did not change significantly after the treatments to be compared.

Catalytic data were measured in a catalytic micro-flow reactor. A total of 100 mg catalyst (250–355 μm) was reduced in two steps, first in diluted H_2 (2% H_2 in He) at a flow rate of 10 N ml min^{-1}, ramping the temperature at 1 K min^{-1} up to 473 K and keeping this temperature for 13.5 h. Then the temperature was increased to 493 K with 1 K min^{-1} and the sample was exposed to pure H_2 at the same flow rate for 0.5 h. Before the activity measurements, the active Cu surface area was determined by N_2O reactive frontal chromatography at room temperature [13]. Methanol synthesis activity was measured at atmospheric pressure both at 493 K and at 473 K in a synthesis gas composed of 72% H_2, 10% CO, 4% CO_2 and 14% He with a flow of 25 N ml min^{-1}. Only data for 473 K will be reported here to make sure that all conversions were measured far from equilibrium (cf. [8]). Analysis of the gas phase was performed by a calibrated quadrupole mass spectrometer (Balzers GAM 422).

3 Results and Discussion

In Fig. 2, the catalytic activity is plotted vs. the Cu surface area determined by the N_2O titration technique (cf. Table 1) for four of our samples and compared with that of the commercial reference catalyst. The Cu surface areas of the former are rather small, which indicates a large particle size, therefore, an inset has been used to include the reference catalyst with its Cu surface area of almost 20 m^2/g. As expected, the model catalysts are much less active than the reference catalyst. The activities were, however, stable during the 24 h test routine, with 21 h at 493 K and 3 h at 473 h.

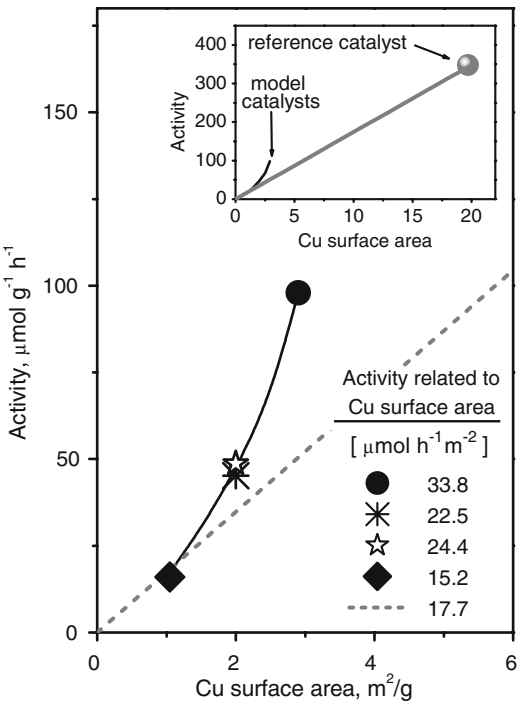

Fig. 2 Dependence of methanol synthesis activity on Cu surface area measured by N_2O reactive chemisorption. Inset—reference catalyst, model catalysts indicated for comparison, main panel—model catalysts, reference catalyst indicated for comparison. $T = 473$ K, synthesis gas consisting of 72% H_2, 10% CO, 4% CO_2 and 14% He, (●) ZnCu-5/14, (✳) ZnCu-3/16, (☆) ZnCu-1/19, (◆) CuZn-15/5, (- - -) reference catalyst

It is known that the methanol synthesis activity is generally proportional to the exposed Cu surface area [3, 4], and that deviations from this proportionality (i.e., variations in the rate per m^2 Cu surface area) can be caused by a more or less pronounced promotion effect of zinc [14]. Figure 2 shows that the rates per m^2 Cu of the model catalysts are comparable to or better than that of the reference catalyst. Therefore, despite the low surface areas and rates it can be concluded that in the model catalysts the efficiency of promotion of Cu by the Zn component is equal to or better than in the reference catalyst Remarkably, the two catalysts with ≈15 wt.% Cu and 5 wt.% Zn are at both ends of the series—CuZn-15/5 is the poorest, ZnCu-5/14 the best catalyst. The reaction rate per m^2 Cu of the latter is twice that of the reference catalyst.

Figure 3 shows the CuK EXAFS spectra (Fourier-transformed, k^2-weighted) of our catalysts, except for ZnCu-1/19 which was omitted due to its very low Zn content. The thin black lines refer to the state after reduction at 523 K. At the first sight, the spectra appear to confirm the conclusion from N_2O adsorption about the large particles size: although the scattering signals are weaker than those of the Cu foil, there is hardly any amplitude decay, all features up to 8 Å are well developed. The analysis of the first shell resulted in Cu–Cu coordination numbers (C.N.) between 9.4 and 10.2, with typical error margins of ±0.4, hence the copper dispersion is roughly the same for all samples measured. According to a geometrical correlation between first-shell C.N. and spherical particle diameter [15], this corresponds to a particle size of 2–2.5 nm, which is on the whole in agreement with the appearance of the EXAFS spectra: in particles of this size, the amplitude decay should be small in the first shells. There is, however, a strong contradiction to the particle sizes estimated from the N_2O adsorption data: the Cu surface areas in Table 1 translate to particle diameters of 30–50 nm (uniform spheres assumed), which is also far beyond the pore size of the matrix. Such discrepancy has been found earlier with catalysts containing Cu/ZnO_x species in MCM-48 [8]. We believe that this is due to contact of copper particles among each other (in polycrystalline aggregates) and with the matrix walls, which might occur as the particle size approaches the pore size and would lead to dramatic shielding effects. We can, however, not completely rule out that the very small primary particles might have been affected by the interaction with N_2O, which will be studied in ongoing research.

Figure 3 shows also the influence of the $R_{CO}673$ treatment on the CuK EXAFS spectra. This somewhat severe treatment has been devised to replace the much longer procedures used in [4] to transform methanol synthesis catalysts into a state with excess activity (e.g., 64 h 10% CO/He at 493 K). In an unconfined methanol synthesis catalyst, heating to 673 K would be expected to cause severe sintering. This is not the case with our matrix-confined Cu/ZnO catalysts. With the exception of ZnCu-3/16 where the Cu dispersion was highest after reduction at 523 K, the short high-temperature treatment did not cause significant changes in the CuK EXAFS spectra, i.e., the primary Cu particle size was not affected.

The ZnK EXAFS spectra of the same samples are depicted in Fig. 4, where spectra of reference compounds (Zn, ZnO) are given as well. After reduction at 523 K (thin

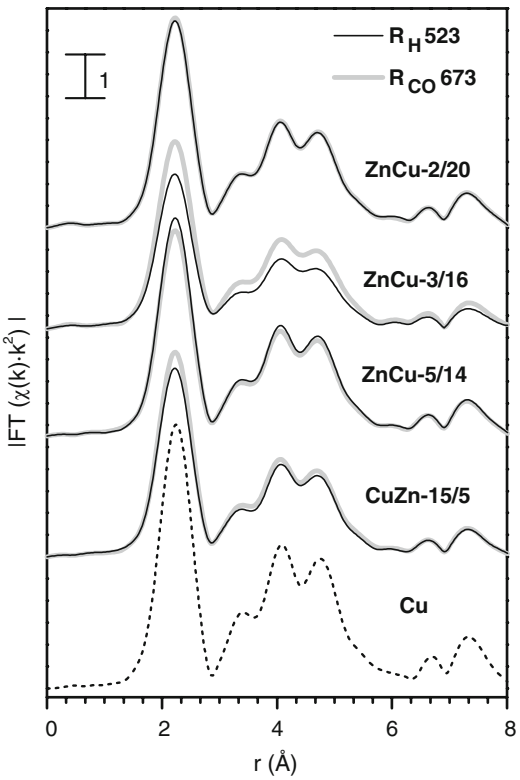

Fig. 3 CuK EXAFS spectra of model catalysts after different pretreatments. R_H523: 15 min H_2 (5% in He) at 523 K, with 5 K/min temperature ramp, $R_{CO}673$: 15 min CO/H_2 (10% CO) at 673 K, after R_H523, with 5 K/min temperature ramp

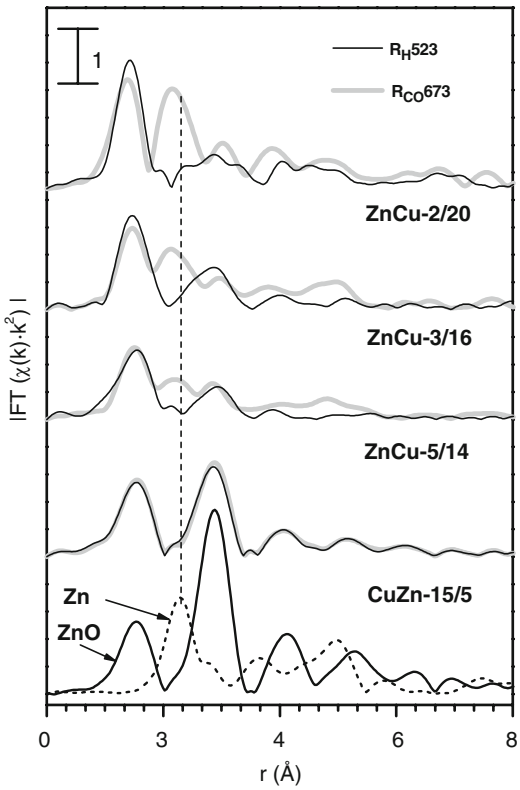

Fig. 4 ZnK EXAFS spectra of model catalysts after different pretreatments. R_H523: 15 min H_2 (5% in He) at 523 K, with 5 K/min temperature ramp, $R_{CO}673$: 15 min CO/H_2 (10% CO) at 673 K, after R_H523, with 5 K/min temperature ramp

black lines), almost all spectra resembled that of bulk ZnO, with scattering features at 1.55 Å (Zn–O, all distances uncorrected) and 2.9 Å (Zn–Zn). At the higher Zn contents, a further shell at ≈4.1 Å could still be discerned. The higher shells were much weaker than in the ZnO spectrum because the particles were small. In ZnCu-2/20, the Zn–Zn shell was no longer significant on an increased noise level, and the Zn–O distance was by ca. 0.1 Å smaller than in ZnO. Apparently, particle formation had not occurred in this sample, which is similar to what has been observed earlier after introduction of zinc via aqueous routes [8]. The difference between the samples with reversed introduction of copper and zinc was pronounced: In CuZn15/5, the Zn–Zn shell of ZnO was well developed whereas it was very weak in ZnCu-5/14.

In three of these samples, treatment in CO/H_2 at 673 K caused major changes in the ZnK EXAFS spectra whereas CuZn-15/5 did not show any effect (grey lines). In the spectra of the remaining samples, a new shell appeared at 2.15 Å, and its intensity increased with decreasing Zn content. There was a further, weak signal at ca. 2.9 Å (probably a residual oxide Zn–Zn coordination) and broad features at ≈3.8 Å and ≈4.9 Å. The first new shell appeared at a smaller distance than the Zn–Zn shell in zinc metal (2.15 vs. 2.30 Å), the higher shells were roughly compatible with those of either zinc (at 3.6 and 5.0 Å) or copper (at 4.0 and 4.75 Å).

The first three shells of these spectra were modelled assuming the second one (X) to arise from a zinc *or* a copper neighbour whereas the first and the third shell were assigned to oxygen and zinc, respectively. The Zn–Cu path was analysed on the basis of a FEFF-8.10 calculation for a cubic Zhangengite structure (Cu:Zn = 1:1). The results for ZnCu-5/14 are given in Fig. 5 and Table 2. The sample has been selected because due to the larger Zn/Cu ratio possible errors due imperfect correction of the Cu influence on the Zn spectrum (*vide supra*) are smallest. Indeed, correction of the spectra with slightly different treatment of the subtracted Cu spectrum did produce some differences, which were naturally most pronounced in the case of ZnCu-2/20. Notably, the uncertainties occurred almost exclusively in the first (Zn–O) shell whereas the further shells (including Zn–X) were well reproduced. Not unexpectedly, in the fitting of ZnCu-5/14, both versions (X = Cu or Zn) gave very similar results (Table 2). The metal neighbour was found at a distance of 2.54–2.55 Å whereas the coordination numbers were ≈1.5. The error margins of these values are rather large, but the shell is clearly significant. The fitting of the first (Zn–O) shell was unsatisfactory as the E_0 parameter tended towards the preset limitation (8.0 eV). We assign this and the increased uncertainties in some of the resulting parameters to the above-mentioned problems with the correction of the spectrum.

For X = Zn, the Zn–Zn distance found was considerably smaller than in bulk Zinc (2.665 Å) which might be explained by the formation of small particles. However, in earlier work with Cu nanoparticles, the contraction of the Cu–Cu distance was never beyond 0.05 Å [16, 17]. Therefore, the experimental Zn–X distance of 2.55 Å favours a Zn–Cu coordination. In both versions, the Zn–O C.N. was somewhat below 3, i.e., smaller than those in ZnO (one O at 1.796 Å, 3 O at 2.042 Å) or in ZnCu-5/14 after R_H523 where 3.8 O atoms were found at a distance of 1.966 Å. Although conclusions from the first (Zn–O) shell should be drawn with caution, this result certainly indicates some reduction of the zinc.

The question if this reduction is real and if it has produced Zn metal may be best answered by inspecting the XANES region. In Fig. 6, ZnK XANES spectra of CuZn-15/5 and ZnCu-2/20 after different treatments are compared with those of ZnO and Zn metal. ZnCu-2/20 has been

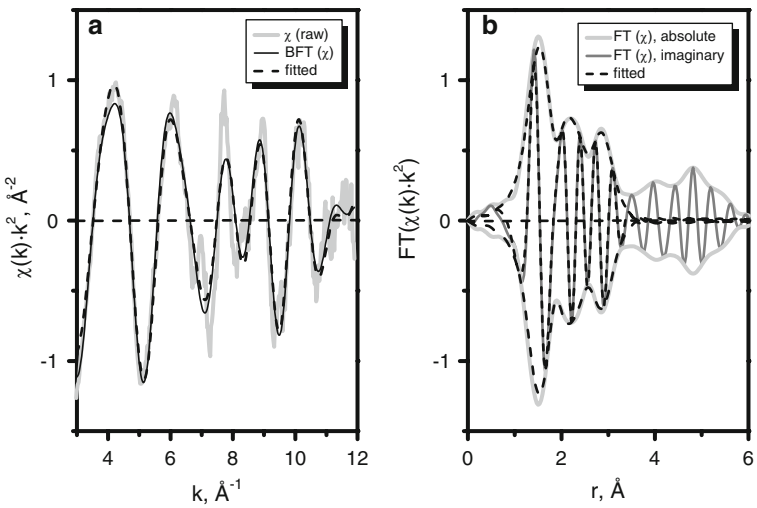

Fig. 5 Best model fit of ZnK EXAFS spectrum of ZnCu5-14 after $R_{CO}673$. **a** k-space, k^2-weighted, (——) raw data, (—) back Fourier-transform, 1.07 < r < 3.25, (- - -) fit of back Fourier-transform, **b** r space, (——) absolute value of Fourier-transform, (▬▬) imaginary part of Fourier-transform, (- - -) fit of absolute value/imaginary part. Numerical values of model in Table 2 (upper part)

Table 2 Model parameters for the fit of the Zn EXAFS of ZnCu-15/4 (cf. Fig. 4)

Shell	r (Å)	C.N.	10^3 σ (Å^{-2})	ΔE_0 (eV)
Zn–O	1.967 ± 0.014	2.8 ± 0.4	4.3 ± 2.3	8.0
Zn–Cu	2.55 ± 0.04	1.4 ± 0.8	4.6 ± 4.0	−2.4
Zn–Zn	3.20 ± 0.04	1.6 ± 1.3	2.8 ± 5.2	−2.1
Zn–O	1.968 ± 0.014	2.6 ± 0.4	3.6 ± 2.3	8.0
Zn–Zn	2.54 ± 0.04	1.5 ± 1.0	5.4 ± 4.3	−1.6
Zn–Zn	3.20 ± 0.04	1.6 ± 1.5	3.2 ± 5.7	−2.0

selected for this comparison instead of ZnCu-5/14 because of the more pronounced effects at lower Zn content. The influence of the adjacent Cu region is marginal in the small XANES energy interval. For ZnCu-2/20, a spectrum taken before reduction is also shown, for CuZn-15/5 it was very close to that after R_H523 and has been therefore omitted.

The XANES of CuZn-15/5 (Fig. 6a) resembled that of ZnO, which exhibits a maximum at 9667 eV with a pronounced shoulder at 9662 eV, a peak at 9679 eV with a pronounced minimum in between. The latter peak indicates a tetrahedral coordination of the zinc while the split white-line structure has been assigned to the presence of different Zn–O coordinations in the first shell [18]. The same signals were present in the XANES of CuZn-15/5, however, with lower excursions at maxima and minima, which is a typical feature of small particles [16, 19], and a more intense low-energy shoulder. The edge was shifted to higher energies by ca. 0.5 eV relative to that of ZnO.

The XANES of ZnCu-2/20 in the as-prepared state was completely different (Fig. 6b). Although the edge shift was comparable to that of CuZn-15/5, the intensity rose more steeply, there was neither a shoulder nor a minimum near the main feature, which was comparable in height but much broader than that of ZnO. Instead of the second peak there was a broad maximum extending to higher energies which suggests that octahedral coordinations may also have been present [18]. This confirms the conclusion about the disordered nature of the zinc oxide phase in this sample drawn earlier from the EXAFS spectrum. Upon reduction, the XANES changed significantly. Although the edge energy (taken at the inflection point) did not vary much, the onset of the step shifted to lower energies and the intensity of the main feature decreased as would be expected for a mixture of Zn metal with the initial disordered zinc oxide species.

The following observations show, however, that zero-valent zinc was most likely not involved in the spectral changes observed. These changes occurred to a significant extent already after the R_H523 treatment, where no indication for the new Zn–X shell can be seen in the EXAFS spectrum (Fig. 4). Such changes can arise from variations in the zinc coordination sphere [18, 20, 21]. The minor edge shift to lower energy and the decreased intensity of the main feature may indeed indicate that a partial reduction, e.g., some loss of oxygen, has really happened [22]. Indeed, the effect of R_{CO}673 following R_H523 was quite similar to the changes seen after this hydrogen treatment: the onset shifted further to lower energies, the peak intensity went on decreasing, the edge energy remained, however, almost constant.

It was nevertheless attempted to reproduce the XANES after R_{CO}673 by a linear combination of those of the initial sample and of Zn metal, without satisfactory results. This is not so much due to the inappropriate use of the spectrum for bulk Zn, which may differ in detail from that of Zn nanoparticles [16, 19], but to the incompatibility of the spectra involved (Fig. 6b). Indeed, above the white line energy, the spectrum of Zn and of ZnCu-2/20 after R_{CO}673 are nearly parallel whereas that of the initial sample decays strongly, which suggests a low weight of the latter, i.e., a very high reduction degree. On the contrary, the small

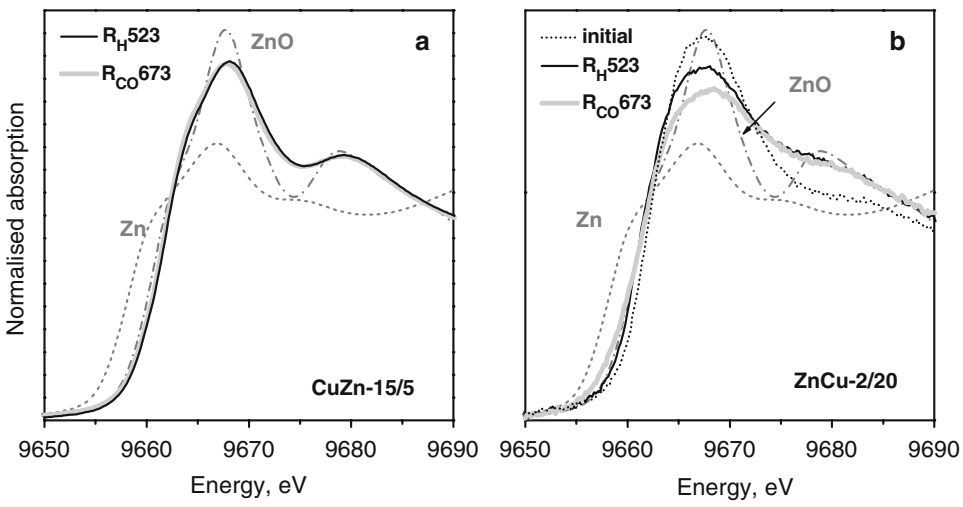

Fig. 6 ZnK XANES spectra of two model catalysts after different pretreatments, compared with data of reference compounds. **a** CuZn-15/5, without new scattering path in the ZnK EXAFS after R_{CO}673 (cf. Fig. 4), **b** ZnCu-2/20, with new scattering path in the ZnK EXAFS after R_{CO}673

effects near the edge onset indicate a low reduction degree whereas equal amounts of both phases would result from the peak height. Therefore, the presence of zerovalent zinc cannot be inferred from the XANES, which shows that the new features in the Zn EXAFS do not arise from Zn metal formation. As mentioned above, this conclusion can be drawn also from the XANES of the remaining samples including ZnCu-5/14. Analogously, EXAFS spectra were simulated by linear combination of k-space spectra of ZnO and Zn and the resulting r-space spectra were compared with those of Fig. 4. It was found that the intensity of the Zn–X shell (X = Zn) fits the experimental data only at reduction degrees of 30–50%, which would cause a much stronger attenuation of the Zn–O shell than observed.

The close neighbourhood of Cu metal atoms and Zn^{2+} ions is at the heart of the Cu–ZnO interaction in methanol synthesis catalysts. The model discussed is in agreement with the concept according to which oxygen deficient ZnO_{1-x} species decorate the surface of the Cu particles under strong reducing conditions [3, 4] causing excess activity by sites at the boundary between them. Inclusion of zinc ions into Cu species [5] would, however, also agree with the appearance of a ZnCu shell in the ZnK EXAFS.

In Fig. 4, it can be seen that intensity of the Zn–Cu shell formed after $R_{CO}673$ increased with decreasing zinc content of the samples. The tendency indicates that the amount of zinc species deactivated by interaction with the siliceous walls was very small in these catalysts prepared from a zinc heterocubane precursor. This is contrary to the case of ZnO_x species introduced by aqueous techniques [8], the ZnK EXAFS spectra of which were very similar to that of ZnCu-2/20 after R_H523 (Fig. 3), arising from a Zn–O shell and a poorly structured feature at larger distance ($\approx$3 Å). However, whereas ZnCu-2/20 developed the Zn–Cu shell upon treatment in CO/H_2 at 673 K (Fig. 4), no changes were seen after such treatment on Cu–ZnO_x/MCM-48 catalysts prepared via aqueous routes [8], which was assigned to the formation of redox inactive zinc silicate species [7]. The presence of a significant amount of zinc species deactivated by the silicate walls would cause the intensity of the Zn–Cu sphere to go through a maximum with decreasing zinc content. Instead, the intensity of this feature went on growing from 3 to 2 wt.% Zn, which indicates that the percentage of deactivated zinc, which would not contribute to this shell, is less than 1.5 wt.%. One may therefore expect that with a larger copper surface area, catalyst states may be achieved in which the overwhelming majority of the zinc present is engaged in the interaction with the copper metal surface. Already in ZnCu-2/20, this percentage was at least 50%. In terms of the zinc inclusion concept (*vide supra*), this would mean that the short reduction treatment $R_{CO}673$, which did not cause significant changes of the copper primary particle size, would have resulted in the inclusion of Zn^{2+} into the Cu particles to an atomic ratio of ca. 1:20. As this seems not very likely, we prefer the decoration concept.

The drastic differences between the two catalysts with equal composition but reverse order of impregnation are surprising, because the initial introduction of Cu had been thought to favour a more intimate mixing between the components. The difference is apparently related to the ZnO particle size which was much smaller when Zn was introduced first. It has been found that the formation of nano-ZnO from the adsorbed heterocubane is a rather sensitive process, which is critically influenced by the water partial pressure during decomposition [23]. It seems that the presence of CuO_x aggregates accelerated the heterocubane decomposition in an undesired manner, maybe due to moisture adsorbed on their polar surfaces.

While our data demonstrate a new approach to monitor dynamical changes in the relation between Cu and ZnO, which were earlier detected more indirectly [3, 4], the significance of these effects for the methanol synthesis activity has yet to be demonstrated. Our data suggest that the ability of zinc to engage in this interaction favours a better activity: indeed, among the catalysts with 5 wt.% Zn and ca. 15 wt.% Cu, the one which developed the Zn–Cu^{2+} interaction upon severe reduction (Zn–Cu-5/14, cf. Fig. 4) was the better catalyst, in particular in terms of rate per m^2 Cu (Fig. 2). It is, however, not clear if or to which extent the interaction indicated by the Zn^{2+}-Cu shell is present under normal reaction conditions. After exposure to dilute CO at 493 K, Wilmer and Hinrichsen observed a gradual decay of the initial excess activity to a stationary state [4], therefore, the catalyst state under stationary reaction conditions will differ from that characterized in the our study. It is for this reason that we did not attempt to relate the activity trends (Fig. 2) with EXAFS features observed (Fig. 4). It remains even to be elucidated if the state achieved after $R_{CO}673$ provides indeed a higher activity than the state after normal reduction, because the treatment differs from those applied in [4]. It is known that over reduction may inflict damage to methanol synthesis catalysts, most likely due to the formation of brass [3], which is, however, unlikely in the states achieved in our study. To characterize the activities in the state with well-developed Zn^{2+}–Cu interaction, *operando* measurements with meaningful measurements of the rather low activities are presently under way.

4 Conclusions

Dynamical changes in the interaction between Cu and ZnO_x have been observed in model methanol synthesis catalysts containing Cu and nanoparticulate ZnO in a

mesoporous silica. Upon severe reduction of such catalysts, a new feature emerged in the ZnK EXAFS spectra, which could be assigned to a Cu neighbour by combined evidence from the ZnK EXAFS and XANES regions. At the same time, the zinc oxide component was partially reduced, but without significant formation of Zn(0). These findings agree with a model according to which substoichiometric ZnO_{1-x} species migrate onto the surface of Cu particles under strongly reducing conditions. Catalysts that developed this Cu–ZnO_{1-x} interaction exhibited a larger methanol synthesis activity per m^2 Cu surface area than a sample in which this interaction did not occur. The observation of the interaction in a sample containing only 2 wt.% Zn suggests that the amount of zinc engaged in undesired interactions with the walls of the SiO_2 matrix is very low in this type of catalyst.

Acknowledgments The work has been funded by the German Science Foundation (DFG) in the framework of the Collaborative Research Center "Metal-Substrate Interactions in Heterogeneous Catalysis" (SFB 558), which is gratefully acknowledged.

References

1. Clausen BS, Schiotz J, Grabaek L, Ovesen CV, Jacobsen KW, Norskov JK, Topsoe H (1994) Top Catal 1:367
2. Hansen PL, Wagner JB, Helveg S, Rostrup-Nielsen JR, Clausen BS, Topsoe H (2002) Science 295:2053
3. Grunwaldt J-D, Molenbroek AM, Topsoe N-Y, Topsoe H, Clausen BS (2000) J Catal 194:452
4. Wilmer H, Hinrichsen O (2002) Catal Lett 82:117
5. Günter MM, Ressler T, Jentoft RE, Bems B (2001) J Catal 203:133
6. Polarz S, Kuschel A (2008) Chem Eur J (in press)
7. Tkachenko OP, Klementiev KV, Löffler E, Ritzkopf I, Schüth F, Bandyopadhyay M, Grabowski S, Gies H, Hagen V, Muhler M, Lu L, Fischer RA, Grünert W (2003) Phys Chem Chem Phys 5:4325
8. Van den Berg MWE, Polarz S, Tkachenko OP, Klementiev KV, Bandyopadhyay M, Khodeir L, Gies H, Muhler M, Grünert W (2006) J Catal 241:446
9. Polarz S, Neues F, van den Berg MWE, Grünert W, Khodeir L (2005) J Am Chem Soc 127:12028
10. Kampers FWH, Maas TMJ, van Grondelle J, Brinkgreve DC, Koningsberger DC (1989) Rev Sci Instrum 60:2635
11. Klementiev KV, VIPER for Windows (Visual Processing in EXAFS Researches), freeware, www.desy.de/~klmn/viper.html
12. Ankudinov AL, Ravel B, Rehr JJ, Conradson SD (1998) Phys Rev B 58:7565
13. Chinchen GC, Hay CM, Vandervell HD, Waugh KC (1987) J Catal 103:79
14. Kurtz M, Bauer N, Büscher C, Wilmer H, Hinrichsen O, Becker R, Rabe S, Merz K, Driess M, Fischer RA, Muhler M (2004) Catal Lett 92:49
15. Borovski M (1997) J Phys IV 7:C2-259
16. Tkachenko OP, Klementiev KV, Van den Berg MWE, Koc N, Bandyopadhyay M, Birkner A, Wöll C, Gies H, Grünert W (2005) J Phys Chem B 109:20979
17. Tkachenko OP, Klementiev KV, van den Berg MWE, Gies H, Grünert W (2005) Phys Chem Chem Phys 8:1539
18. Takahashi M, Tanida H, Kawaguchi S, Harada M, Watanabe I (1999) J Synchrotron Radiat 6:278
19. Bazin DC, Sayers DA, Rehr JJ (1997) J Phys Chem B 101:1140
20. Larcheri S, Armellini C, Rocca F, Kuzmin A, Kalendarev R, Dalba G, Graziola R, Purans J, Pailharey D, Jandard F (2006) Superlattices Microstruct 39:267
21. Zhao W, Chu WS, Yang FF, Yu MJ, Chen DL, Guo XY, Zhou DW, Shi N, Marcelli A, Niu LW, Teng MK, Gong WM, Benfatto M, Wu ZY (2007) Nucl Instrum Methods Phys Res A 580:451
22. Koningsberger DC, Ramaker DE (2008) In: Ertl G, Knözinger H, Schüth F, Weitkamp J (eds) Handbook of heterogeneous catalysis, 2nd edn. VCH, Weinheim, p 774
23. Lizandara C, van den Berg MWE, De Toni A, Goes T, Polarz S (in press) J Am Chem Soc